Optimization of Prosthetic Foot Stiffness to Reduce Metabolic Cost and Intact Knee Loading During Below-Knee Amputee Walking: A Theoretical Study

Nicholas P. Fey
Department of Mechanical Engineering,
The University of Texas at Austin,
Austin, TX 78712

Glenn K. Klute
Department of Veterans Affairs,
Puget Sound Health Care System,
Seattle, WA 98108

Richard R. Neptune[1]
Department of Mechanical Engineering,
The University of Texas at Austin,
Austin, TX 78712
e-mail: rneptune@mail.utexas.edu

Unilateral below-knee amputees develop abnormal gait characteristics that include bilateral asymmetries and an elevated metabolic cost relative to non-amputees. In addition, long-term prosthesis use has been linked to an increased prevalence of joint pain and osteoarthritis in the intact leg knee. To improve amputee mobility, prosthetic feet that utilize elastic energy storage and return (ESAR) have been designed, which perform important biomechanical functions such as providing body support and forward propulsion. However, the prescription of appropriate design characteristics (e.g., stiffness) is not well-defined since its influence on foot function and important in vivo biomechanical quantities such as metabolic cost and joint loading remain unclear. The design of feet that improve these quantities could provide considerable advancements in amputee care. Therefore, the purpose of this study was to couple design optimization with dynamic simulations of amputee walking to identify the optimal foot stiffness that minimizes metabolic cost and intact knee joint loading. A musculoskeletal model and distributed stiffness ESAR prosthetic foot model were developed to generate muscle-actuated forward dynamics simulations of amputee walking. Dynamic optimization was used to solve for the optimal muscle excitation patterns and foot stiffness profile that produced simulations that tracked experimental amputee walking data while minimizing metabolic cost and intact leg internal knee contact forces. Muscle and foot function were evaluated by calculating their contributions to the important walking subtasks of body support, forward propulsion and leg swing. The analyses showed that altering a nominal prosthetic foot stiffness distribution by stiffening the toe and mid-foot while making the ankle and heel less stiff improved ESAR foot performance by offloading the intact knee during early to mid-stance of the intact leg and reducing metabolic cost. The optimal design also provided moderate braking and body support during the first half of residual leg stance, while increasing the prosthesis contributions to forward propulsion and body support during the second half of residual leg stance. Future work will be directed at experimentally validating these results, which have important implications for future designs of prosthetic feet that could significantly improve amputee care. [DOI: 10.1115/1.4007824]

Keywords: biomechanics, gait, transtibial amputee, energy storage and return, forward dynamics simulation

Introduction

Unilateral below-knee amputees have distinct gait characteristics compared to non-amputees, including bilateral asymmetries (e.g., Ref. [1]), altered residual leg muscle activity (e.g., Ref. [2]), increased metabolic cost (e.g., Ref. [3]), and reduced walking speed (e.g., Ref. [4]). As a result, amputees often develop chronic leg and back pain [5–8]. Sustained prosthetic use has also been linked to joint pain in the intact leg knee that is often associated with osteoarthritis (for review, see Ref. [9]). Two of the more prominent biomechanical factors that adversely affect amputee mobility are an elevated metabolic cost and the development of joint disorders in the intact knee.

Differences in gait characteristics between amputees and non-amputees are often attributed to the functional loss of the residual leg ankle muscles, which perform important biomechanical functions such as providing body support, forward propulsion, and leg swing initiation [10]. Passive prosthetic devices such as energy storage and return feet have been developed to help improve amputee gait by storing and releasing elastic energy during stance [11]. However, selection of the appropriate foot design (e.g., stiffness characteristics) is not well-defined since its influence on ESAR foot function and biomechanical quantities such as metabolic cost and joint loading (e.g., knee contact forces) are not well-understood.

A promising strategy to optimize ESAR foot design and prescription practice is to combine design optimization with advanced manufacturing techniques such as selective laser sintering (SLS) to develop novel designs that improve these important biomechanical quantities. However, it is essential to identify the dynamic interactions between the musculoskeletal system and the design characteristics of the prosthetic foot to assess their influence on walking performance. Therefore, the purpose of this study was to couple design optimization of ESAR prosthetic feet with forward dynamics simulations of amputee walking to identify the

---

optimal foot designs that improve metabolic cost and joint loading during below-knee amputee walking.

In previous applications, forward dynamics simulations have been useful in assessing individual muscle function (e.g., Refs. [12,13]) and estimating difficult to measure *in vivo* quantities such as muscle work, metabolic cost, and joint contact forces during human movement (e.g., Refs. [14–18]). In addition, studies have shown how altering the stiffness of prosthetic foot-ankle devices can have a significant influence on the walking mechanics and muscle activity of below-knee amputees [19–21]. Thus, we expect that altering foot stiffness likely influences metabolic cost and joint contact forces and that there is an optimal foot stiffness that minimizes these quantities. In order to interpret how changes in stiffness influence muscle and prosthetic foot function, individual muscle and foot contributions to body support, forward propulsion, and residual leg swing were determined.

Methods

Musculoskeletal Model. An amputee (left leg below -knee) planar bipedal musculoskeletal model was developed using SIMM/Dynamics Pipeline (MusculoGraphics, Inc.), which was similar to the model used in previous studies of amputee and non-amputee walking (e.g., Ref. [10,22], (Fig. 1).

Rigid segments represented the trunk (head, arms, and torso) and thigh and shank segments of both legs. In the intact leg foot, rigid segments also represented the talus, calcaneus, mid-foot, and toes. The musculoskeletal geometry was based on Delp et al. [23], while the inertial properties of the residual leg shank segment were adjusted based on the work of Mattes et al. [24]. The trunk had three degrees-of-freedom (two translations and one rotation). In both legs, hip flexion/extension was modeled using revolute
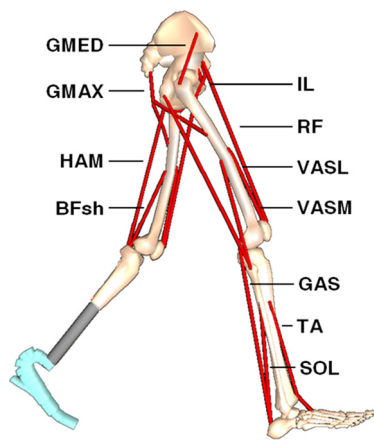

Fig. 1 Amputee musculoskeletal model. The intact leg was actuated by 25 individual Hill-type musculotendon actuators, which were grouped into 14 muscle groups based on anatomical classification with muscles in each group receiving the same excitation pattern. The 14 muscle groups consisted of GMED (anterior and posterior compartments of the gluteus medius), GMAX (gluteus maximus, adductor magnus), HAM (biceps femoris long head, medial hamstrings), BFsh (biceps femoris short head), IL (psoas, iliacus), RF (rectus femoris), VASL (vastus lateralis, vastus intermedius), VASM (vastus medialis), GAS (medial and lateral gastrocnemius), SOL (soleus, tibialis posterior), TA (tibialis anterior, peroneus tertius), PR (peroneus longus, peroneus brevis), FLXDG (flexor digitorum longus, flexor hallucis longus), and EXTDG (extensor digitorum longus, extensor hallucis longus). To improve model visualization, the smaller muscle groups that actuated the foot (PR, FLXDG, and EXTDG) are not shown. In the amputee residual leg, the same muscle groups were included except for those crossing the ankle joint (GAS, SOL, TA, PR, FLXDG, and EXTDG).

joints. A planar joint was used to model the knee joint, with the flexion/extension rotation and two translational degrees-of-freedom prescribed as a function of knee flexion angle [25]. In the intact leg, revolute joints modeled the ankle, subtalar, and metatarsophalangeal joints. Excluding the prosthetic foot, the musculoskeletal model had a total of ten degrees-of-freedom. The dynamical equations of motion were generated using SD/FAST (PTC) while the foot-ground contact was modeled using 31 viscoelastic elements with Coulomb friction under each foot [26]. Passive torques were applied at each joint representing ligaments, passive tissue and joint structures [27,28].

Musculotendon Actuators. Muscles were modeled using Hill-type actuators, which consisted of a contractile element representing the active muscle fibers, series elastic element representing the tendon, and parallel elastic element representing the passive fiber stiffness. Similar to previous work [29], the excitation pattern of each actuator was defined using a bimodal pattern defined as

$$e(t) = \sum_{i=1}^{2} \begin{cases} \frac{a_i}{2}\left[1 - \cos\left(\frac{2\pi(t - \text{onset}_i)}{\text{offset}_i - \text{onset}_i}\right)\right], & \text{onset}_i \leq t \leq \text{offset}_i \\ 0, & \text{otherwise} \end{cases}$$

where the excitation magnitude e(t) was a function of time (t) and amplitude (a_i), onset (onset_i) and offset (offset_i) of each mode (i). Thus, six parameters (two onsets, offsets, and amplitudes) defined the excitation pattern of each muscle group. Muscle contraction dynamics were governed by force-length, force-velocity, and tendon force-strain relationships [30]. Muscle activation-deactivation dynamics was modeled by a first-order differential equation [31], with activation and deactivation time constants derived from Winters and Stark [32]. For those muscles not included in Winters and Stark [32], nominal activation and deactivation time constants of 12 and 48 ms were used.

Metabolic Cost and Joint Contact Forces. The metabolic cost model was based on previous work [18,33] and included thermal and mechanical energetic costs. Modifications were made to the original model such that slow-twitch muscle fibers were recruited prior to fast-twitch fibers. Energy liberation rate for each muscle ($\dot{E}$) was the sum of activation ($\dot{h}_A$), maintenance ($\dot{h}_M$), and shortening/lengthening ($\dot{h}_{SL}$) heat rates, as well as the mechanical work rate ($\dot{w}_{CE}$) of the contractile element. Mechanical work rate ($\dot{w}_{CE}$) was the product of the contractile element's force and velocity. Total energy consumption for each simulation was calculated by the time integral of the energy liberation rate over the gait cycle defined as:

$$\dot{E} = \dot{h}_A + \dot{h}_M + \dot{h}_{SL} + \dot{w}_{CE}$$

In addition, the total knee tibiofemoral and hip contact forces were calculated using SD/FAST, which included the intersegmental forces and compressive forces due to the muscles spanning the joint.

Energy Storage and Return Prosthetic Foot Model. The prosthetic foot model consisted of 22 rigid segments. Each segment and the overall foot shape were defined by two spline curves that represented the keel and heel sections (Fig. 2). The keel and heel shapes were defined using 15 and 9 spline points, respectively. This shape was used since it closely matched the shape of a widely-prescribed commercial carbon fiber ESAR foot (Highlander^{TM}, FS3, Freedom Innovations, LLC) and was previously used to generate prototypes of ESAR prosthetic feet using selective laser sintering [19,34]. The prosthetic foot model had a total of 18 degrees-of-freedom (13 keel and 5 heel single degree-of-freedom revolute joints, Fig. 2). Individual keel elements were aggregated
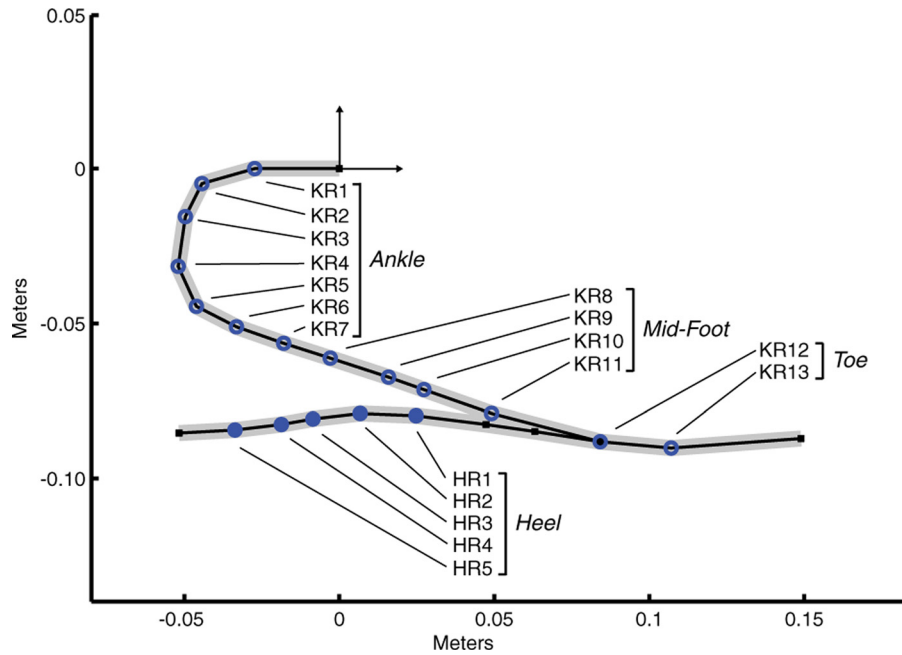
Fig. 2 Schematic of the prosthetic foot model consisting of 22 rigid segments connected in series. The prosthetic foot model had 13 keel (KR1–KR13, ○) and 5 heel (HR1–HR5, ●) rotational degrees-of-freedom. Foot stiffness was modeled using viscoelastic elements at each rotational degree-of-freedom.

Table 1 Metabolic cost and intact knee contact force objectives. Minimizing intact knee contact force sought to minimize the peak magnitude and impulse (integrated force over the entire gait cycle) of the axial component of the knee contact force. Also included in this table are the optimized scale factors, which varied the prosthetic foot stiffness distribution. Bold numbers in the table highlight similarities in metabolic cost and intact knee contact force objectives as well as optimized scale factors across columns.

	Min (MetE)	Min (JCont + MetE)	Min (JCont)
Metabolic cost (J)	**307**	**315**	481
Intact kneel imp. (N*s)	1389	**1130**	**1062**
Intact knee peak (N)	3473	**2424**	**2480**
Prosthetic ankle scale	**0.81**	**0.83**	1.07
Prosthetic mid-foot scale	**1.86**	**1.88**	**1.97**
Prosthetic toe scale	0.5	**1.99**	**1.83**
Prosthetic heel scale	**0.5**	**0.55**	**0.5**

for analysis purposes into an ankle, a mid-foot, and a toe (seven, four, and two joints, respectively).

Prosthetic Foot Stiffness. Foot stiffness was modeled using viscoelastic elements at each rotational degree-of-freedom in the prosthetic foot model, which applied a passive torque in the following form:

$$\tau_i = -k_i \cdot \theta_i - b \cdot \dot{\theta}_i$$

The passive torque (τ_i) applied at each rotational degree-of-freedom (i) was a function of element stiffness (k_i), angular displacement (θ_i) and angular velocity ($\dot{\theta}_i$). A damping value b = 5.73 N*m*s was determined based on previous work [19].

Dynamic Optimization. A simulated annealing optimization algorithm [35] was used to generate three simulations of a complete gait cycle of amputee walking in which prosthetic foot stiffness (four stiffness parameters), muscle excitation parameters
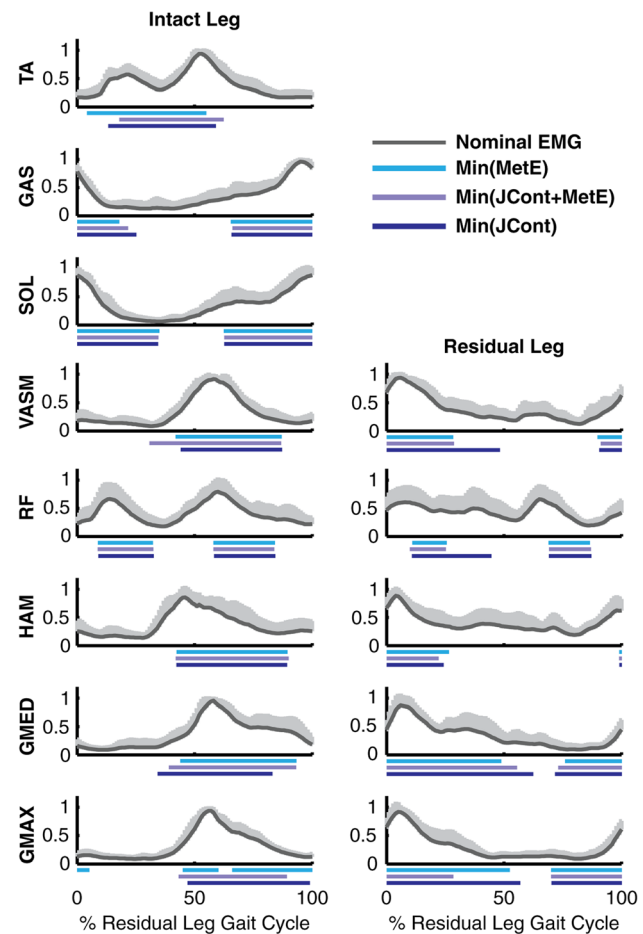

Fig. 3 Comparison of simulation excitation timing (plotted below each x-axis) with group average experimental EMG data (+1 SD) of amputee subjects walking with the SLS ESAR foot plotted with respect to the residual leg gait cycle (only those muscles in which EMG data were collected are shown)
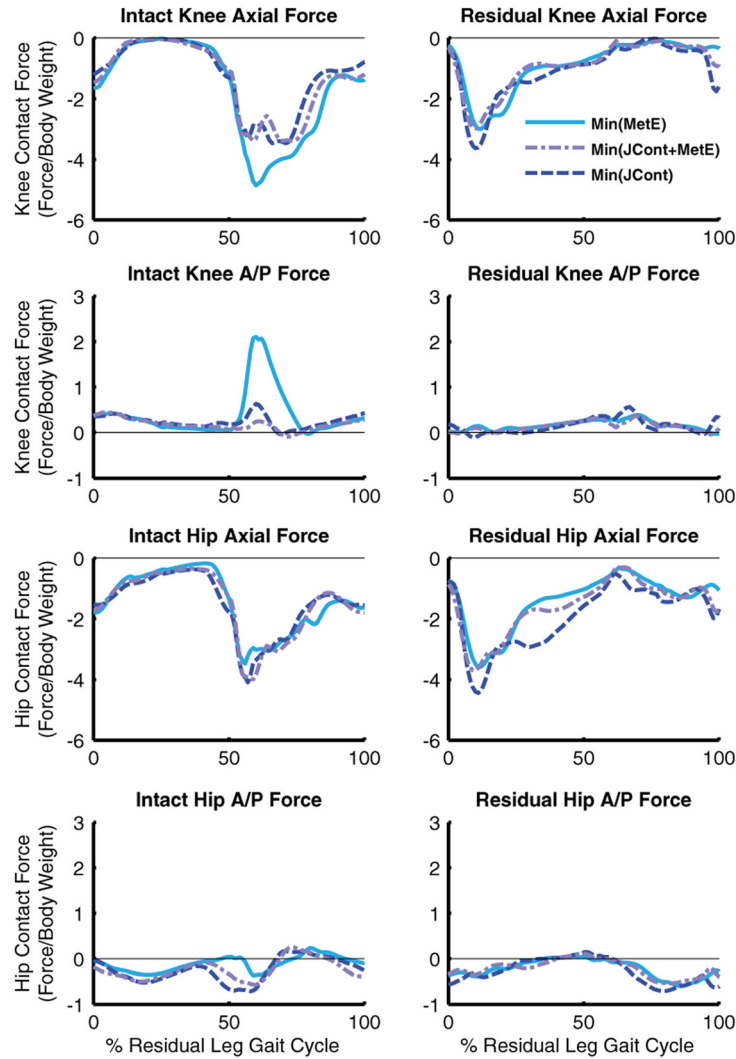
Fig. 4 Intact and residual knee and hip contact forces for each walking simulation plotted with respect to the residual leg gait cycle. For each joint, forces are expressed in the distal segment reference frame and represent the force of the proximal segment on the distal segment. For example, the intact knee axial force is expressed in the intact leg tibia reference frame and represents the force of the intact femur on the intact tibia. Segment reference frames are defined to be positive in the vertical axial direction and positive in the anterior horizontal direction. The total body weight of the model was 715 N.

(six bimodal parameters in each of the 22 muscle groups), and initial generalized velocities (28 velocity parameters, one for each degree-of-freedom) for a total of 164 parameters were optimized to reproduce group average amputee experimental data while: (1) minimizing metabolic cost, (2) minimizing intact knee contact force (equally weighted absolute sum of the peak axial knee contact force and axial knee contact force impulse), and (3) minimizing both metabolic cost and intact knee loading (equally weighted).

To provide an initial guess for prosthetic foot stiffness, a nominal stiffness distribution was calculated based on a custom ESAR foot that was manufactured using SLS and previously shown to closely match the stiffness and biomechanical response of the Highlander[TM] FS3 [34]. Each prosthetic foot segment was assumed to be a prismatic beam element and made from Rilsan[TM] D80 (Nylon 11, Arkema, Inc.) material. The rotational stiffness of each element (KR1–KR13 and HR1–HR5, Fig. 2) was calculated as follows:

$$k_i = \frac{E \cdot I_i}{L_i}$$

The rotational stiffness (k_i) was a function of the Young's modulus of the sintered Nylon 11 material used to manufacture the SLS ESAR prosthetic foot (E = 1.4 GPa), segment length (L_i) and area moment of inertia for a rectangular cross-section (I_i). In the optimization framework, foot stiffness distribution was altered by four scale factors, which independently scaled the ankle (KR1–KR7), mid-foot (KR8–KR11) and toe (KR12 and KR13) sections of the keel in addition to the heel (HR1–HR5). Initial scale factors (ankle, mid-foot, toe and heel sections) were set to 1.0.

Experimental Tracking Data. To provide tracking data for the dynamic optimization, previously collected experimental data of amputees walking with the SLS ESAR foot were used [19]. Subjects provided informed consent to an Institutional Review Board approved protocol and included 12 unilateral, below-knee amputees (10 traumatic, 2 secondary illness; 12 males; 52 ± 17 years; 83.0 ± 15.8 kg; 1.78 ± 0.06 m). Each subject walked along a 10 m walkway at 1.2 (± 0.06) m/s. Bilateral kinematic marker data [36] were measured at 120 Hz using an eight-camera motion
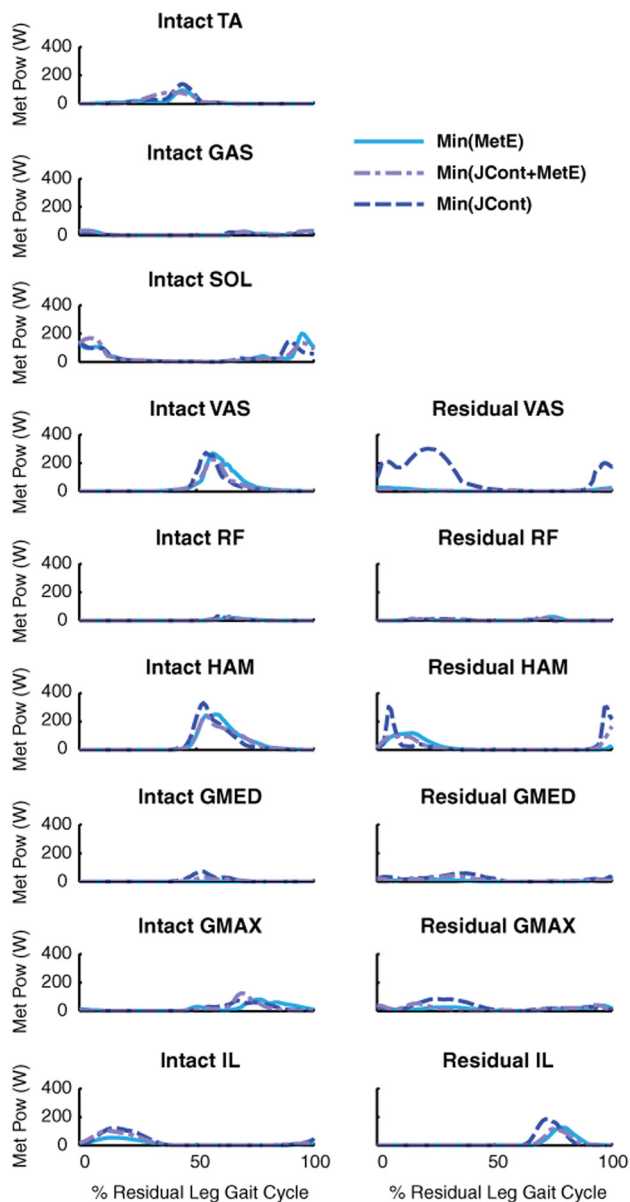
Fig. 5 Metabolic cost profiles of the intact and residual leg muscle groups with the largest contributions plotted with respect to the residual leg gait cycle. VASL and VASM values were combined (VAS). All others had minimal values.

capture system (Vicon, Oxford Metrics, Inc.), and ground reaction force (GRF) data were measured at 1200 Hz using four embedded force plates (Advanced Mechanical Technology, Inc.). Repeated trials were collected until at least five step-to-step force plate contacts per foot were measured. Surface electromyography (EMG) electrodes (2, 10 mm disposable self-adhesive Ag/AgCl sensor contacts, 16 mm interelectrode distance; TeleMyo 900, Noraxon U.S.A., Inc.) were used to record muscle activity from the intact leg tibialis anterior, soleus, medial gastrocnemius, and bilaterally from the vastus medialis, rectus femoris, biceps femoris long head, gluteus maximus and gluteus medius.

Muscle and Prosthetic Foot Function. To compare differences in muscle and foot function between the simulations, individual muscle and foot contributions to body support, forward propulsion, and residual leg swing were calculated using a GRF decomposition [10,13,37] and induced acceleration and segment power analyses [38]. Body support and forward propulsion were quantified by their contributions to the vertical and

anterior/posterior (A/P) GRFs, respectively. Contributions to residual leg swing were quantified by the mechanical power delivered to the residual leg during swing by muscles and the prosthetic foot.

Results

Minimization of Metabolic Cost and Intact Knee Contact Force. The simulations that minimized only metabolic cost (MetE) and only intact knee contact force (JCont) successfully reduced each objective function (Table 1) while the simulation that minimized both metabolic cost and intact knee contact force (JCont + MetE) successfully reduced both functions, which were comparable to the two individually-minimized simulation magnitudes. While the optimized stiffness scale factors varied, there were notable similarities in the stiffness factors across simulations (Table 1). Simulations that minimized metabolic cost decreased ankle stiffness by approximately the same amount and all simulations increased mid-foot stiffness. Mid-foot stiffness was increased the most when minimizing intact knee contact force. Minimizing only metabolic cost decreased toe stiffness, while minimizing intact knee contact force increased toe stiffness. All simulations decreased heel stiffness.

Experimental Tracking Data. Despite the altered stiffness profiles of the prosthetic feet, each simulation produced movements that were similar to the collected experimental data. Across all simulations, average root-mean-square kinematic joint angle and ground reaction force tracking deviations were 8.9 deg and 0.09 GRF/BW, respectively, which were ~2 standard deviations of the experimental data (9.0 deg and 0.08 GRF/BW). For the muscle groups in which experimental EMG data were collected, the optimized excitation patterns were similar and active during regions of the gait cycle when EMG activity was observed (Fig. 3).

Joint Contact Forces and Muscle Contributions to Metabolic Cost. In the simulations that minimized the intact leg knee axial force, the intact knee A/P contact force was decreased relative to minimizing only metabolic cost (Fig. 4). However, small increases of the intact hip axial and A/P contact force during the same region of the gait cycle were observed. In the simulation that minimized only intact knee axial force, increased residual leg knee and hip axial forces were observed compared to the other simulations. In the simulations that minimized metabolic cost, several residual (VAS, HAM, GMED, GMAX and IL) and intact (TA, HAM, GMED and IL) leg muscles showed decreases in metabolic cost (Fig. 5).

Prosthesis Foot Contributions to Body Support and Forward Propulsion. During the first half of residual leg stance when minimizing metabolic cost, the keel provided more braking and body support while muscles provided less body propulsion (Figs. 6(a) and 6(c)). In contrast, when minimizing only intact knee contact force, the keel provided less braking and body support, while the heel provided more braking and support (Figs. 6(a) and 6(c)).

During the second half of residual leg stance when minimizing only metabolic cost, the keel provided less forward propulsion (Fig. 6(b)). When minimizing only intact knee contact force, the keel provided a moderate amount of forward propulsion while muscles provided more propulsion. When minimizing both objectives, the keel provided the most forward propulsion and body support, while muscle contributions to these tasks were moderate (Figs. 6(b) and 6(d)).

Over the entire residual leg stance, minimizing only intact knee contact force required greater muscle contributions to propulsion (Figs. 6(a) and 6(b)).

Individual Muscle Contributions to Body Support and Forward Propulsion. When minimizing only intact knee contact force, throughout stance the residual leg GMED and GMAX

0-50% Residual Stance

(A)

50-100% Residual Stance

(B)

- Min(MetE)
- Min (MetE+JCont)
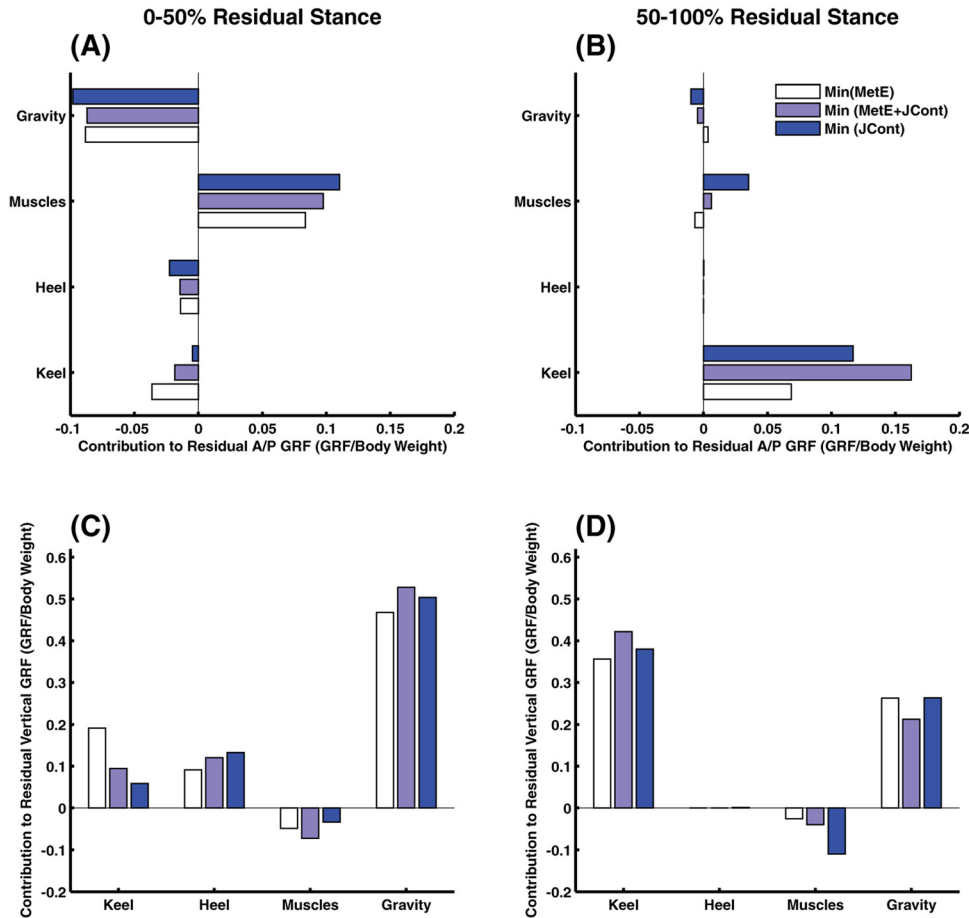- Min (JCont)

(C)

(D)

Fig. 6 Mean contributions of the prosthetic keel and heel, muscles (residual *and* intact legs), and gravity to residual leg A/P and vertical ground reaction forces during the first (left column) and second (right column) halves of residual leg stance

increased their contributions to forward propulsion (Figs. 7(*a*) and 7(*b*)). In addition, during the first half of stance, the residual HAM increased its contribution to body support and decreased its contribution to propulsion (Figs. 7(*a*) and 7(*c*)).

During the first half of intact leg stance in all three simulations, the intact leg RF, VAS, GAS, and SOL provided braking, while HAM provided forward propulsion (Fig. 8(*a*)). The intact leg RF, VAS and HAM contributions to braking and propulsion during this region followed consistent trends in which the simulation that minimized only metabolic cost had the largest contributions, the simulation that minimized only intact knee contact force had the second largest contributions, and the simulation that minimized both objectives had the smallest contributions (Fig. 8(*a*)). Also during the first half of intact leg stance in all three simulations, the intact leg GMED, HAM, VAS, GAS, and SOL had the highest contributions to body support (Fig. 8(*c*)). While minimizing intact knee contact force, GMED and SOL increased their contributions. When minimizing both objectives, the contribution of VAS to body support was largely decreased, and the contribution of HAM was largely increased. In contrast, when minimizing only metabolic cost, the contribution of intact VAS to body support was largely increased (Fig. 8(*c*)).

During the second half of intact leg stance, the primary contributors to body support and forward propulsion were SOL and GAS (Figs. 8(*b*) and 8(*d*)). When minimizing only intact knee contact force, GAS contributions to support and propulsion were decreased, while SOL contributions to forward propulsion were increased. When minimizing both objectives, SOL contributions to propulsion and support decreased.

Prosthesis Foot and Muscle Contributions to Residual Leg Swing. Across simulations, the largest differences in power delivered to the residual leg occurred in the second half of stance during pre-swing (Fig. 9(*b*)). When minimizing only metabolic cost, the prosthetic keel absorbed less energy from the residual leg. When minimizing only intact knee contact force, the keel absorbed greater energy from the residual leg. When reducing only intact knee contact force, residual GMED, GMAX, and RF absorbed more energy from the leg. When minimizing both objectives, the residual leg RF absorbed the least amount of energy from the leg. Lastly, when minimizing only intact knee contact force, during swing the residual leg IL delivered more energy to the leg (Fig. 9(*c*)).

Discussion

The purpose of this study was to couple design optimization with forward dynamics simulations of amputee walking to identify the optimal prosthetic foot design that minimizes the biomechanical quantities of metabolic cost and intact leg loading. We hypothesized that optimal foot stiffness characteristics exist that minimize metabolic cost and intact knee joint contact forces. Integrating prosthetic foot design optimization with forward dynamics simulations enabled us to not only examine the performance of ESAR foot designs but also the interactions between foot and muscle contributions to essential walking subtasks of body support, forward propulsion, and leg swing. The results showed that there are indeed foot stiffness characteristics for unilateral below-knee amputees that minimize metabolic cost and intact knee

0-50% Residual Stance

(A)

50-100% Residual Stance

(B)

Legend: Min(MetE), Min (MetE+JCont), Min (JCont)
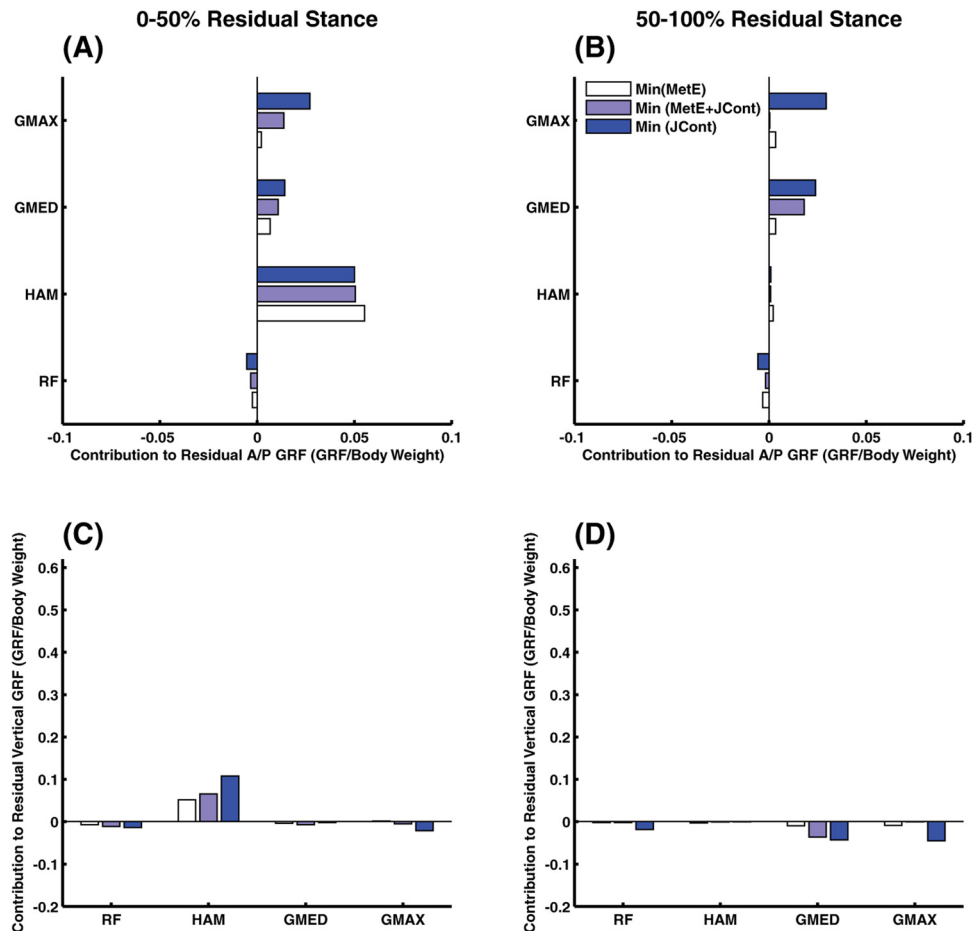
(C)

(D)

Fig. 7 Mean residual leg muscle contributions to A/P and vertical GRFs of the residual leg. Data were averaged during the first (left column) and second (right column) halves of residual leg stance.

contact forces. In addition, there were interesting tradeoffs in foot and muscle function.

Reducing Metabolic Cost. When minimizing only metabolic cost, reducing ankle stiffness, toe stiffness, and heel stiffness, while increasing mid-foot stiffness was the optimal ESAR foot design. This decreased the total muscle contributions to residual leg braking and propulsion throughout residual leg stance and decreased the keel contribution to forward propulsion during the second half of stance. However, minimizing only metabolic cost increased the dependence on the keel during the first half of residual leg stance for body support, and dramatically increased intact leg VAS contributions to body support during the first half of intact leg stance. In addition, the keel absorbed much less energy from the residual leg during the second half of stance, thus requiring less energy delivered to the leg by IL during swing. Therefore, this keel design decreased the overall metabolic demand from muscles of both legs.

However, this ESAR foot design led to increased intact knee loading (highest axial and A/P contact forces), primarily from increased contributions of the intact leg VAS. VAS has been shown to be a primary contributor to the axial knee contact force during non-amputee walking [16]. The peak axial intact knee force (∼3500 N) was largely increased compared to the residual leg knee in this simulation (∼2100 N) as well as compared to previous simulation analyses of non-amputee walking at the same speed (∼2100 N) [16] and other moderate speeds (∼1600–2000 N) [17,39,40]. Also, in an experimental study of amputee walking, as overall ESAR foot stiffness was decreased, increased activity of

the intact leg VAS muscles was observed [19]. Thus, reducing ankle or toe stiffness leads to increases in VAS muscle activity and a substantial increase in intact knee loading.

Reducing Intact Knee Contact Force. When minimizing only intact knee contact force, maintaining ankle stiffness while increasing mid-foot and toe stiffness and decreasing heel stiffness was the optimal ESAR foot design. This enabled the keel to provide a moderate amount of forward propulsion during the second half of residual leg stance but increased the total muscle contributions to residual leg propulsion throughout stance. Increased contributions to forward propulsion by residual leg GMAX and GMED as well as the highest contributions of intact SOL to forward propulsion were observed. Minimizing only intact knee contact force also decreased the dependence on the keel for residual leg body support and increased the dependence on residual HAM to provide support during the first half of stance (Fig. 7(c)). Increased residual leg HAM activity during the first half of stance has been found to be one of the most consistent compensations used by unilateral below-knee amputees during walking (e.g., Ref. [2]). Therefore, increasing the HAM demand may present an increased risk of fatigue or increase the already elevated metabolic cost of amputee walking (see residual leg HAM, Fig. 5).

During the second half of intact leg stance, the smallest contributions of intact GAS to forward propulsion and body support were observed, which were consistent with reducing the intact knee contact force since GAS has been shown to be the primary contributor to axial knee contact force during the second half of stance [16]. This keel design also absorbed the largest energy
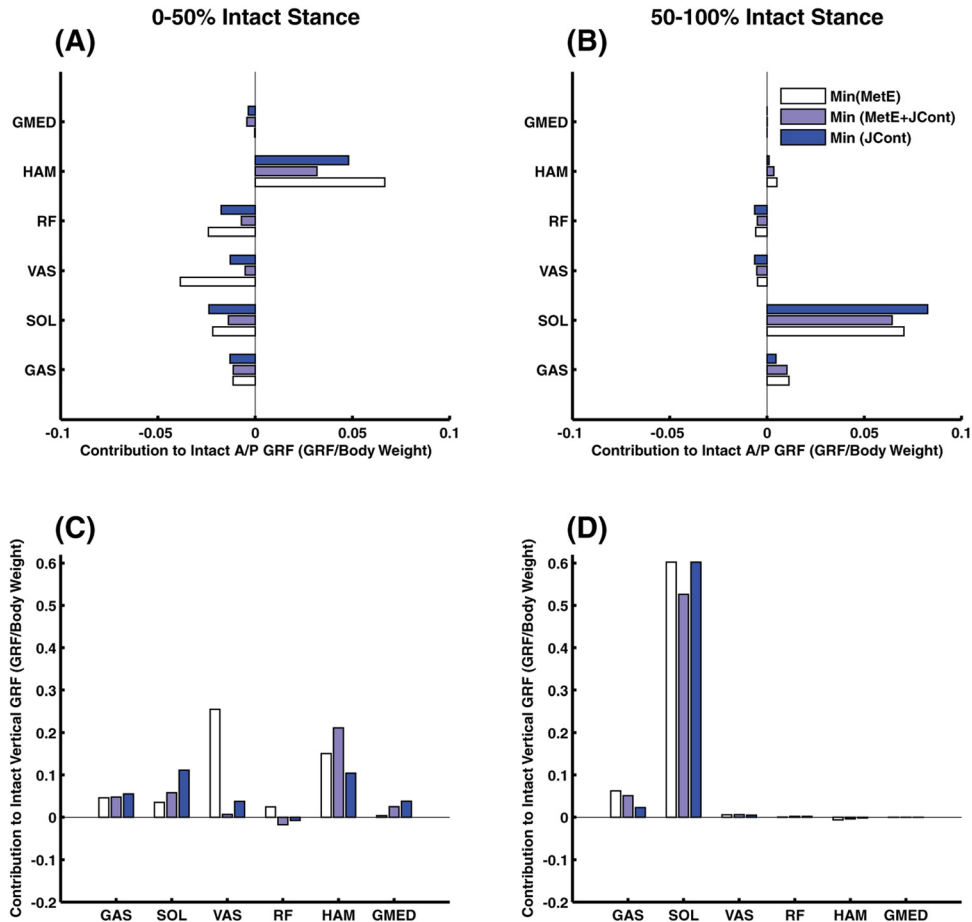
Fig. 8 Mean intact leg muscle contributions to A/P and vertical GRFs of the intact leg. Data were averaged during the first (left column) and second (right column) halves of intact leg stance. Contributions of VASL and VASM were combined (VAS) for presentation of these data.

from the leg during the second half of residual leg stance (Fig. 9(b)), which required a small increase in the energy delivered by IL to the leg during swing (Fig. 9(c)). These changes in foot and muscle function resulted in a higher overall metabolic cost of walking. Thus, while this keel design successfully offloaded the intact knee (by reducing both axial and A/P contact forces in the intact knee), it required an increase in metabolic cost and resulted in higher contact forces of the other lower limb joints (i.e., increased axial forces in the intact hip and residual knee and hip joints), with axial knee forces being similar in both the intact and residual joints (~2500 N). However, these values were still substantially higher than predicted peak knee axial forces during normal non-amputee walking at the same speed (~2100 N) [16] and other moderate speeds (~1600–2000 N) [17,39,40].

Reducing Both Metabolic Cost and Intact Knee Contact Force. When minimizing both metabolic cost and intact knee contact force, the prosthetic keel design encompassed design aspects of the individual optimizations. Ankle stiffness was decreased (similar to when minimizing only metabolic cost), and toe stiffness was increased (similar to when minimizing only intact knee contact force). Mid-foot stiffness was also increased while heel stiffness was again decreased. This optimal ESAR foot design produced the most forward propulsion and body support during the second half of residual leg stance, as well as moderate braking and body support during the first half of stance. This keel design also largely decreased the contributions of the intact SOL to forward propulsion and body support during the second half of intact leg stance. In addition, contributions of the intact VAS to body support during the first half of intact leg stance were largely

decreased and led to a decrease in the intact knee axial force. To compensate for decreased intact VAS function, intact HAM contributions to body support were increased. HAM contributions to the knee axial force have been shown to be much less than VAS during walking [16]. Therefore, this keel design enabled the model to offload the intact leg knee and led to a decreased metabolic cost of walking. However, changes in both prosthetic keel and muscle function were essential.

Offloading the intact leg knee by limiting the contributions of VAS is consistent with previous modeling work that suggested a quadriceps avoidance gait pattern may be used by non-amputee patients that experience knee osteoarthritis [16]. Osteoarthritic non-amputee patients typically experience decreased knee flexion angles and knee extensor torques during early stance [41–44]. Other studies have suggested that an increased dependence on HAM over VAS may be an effective method to mitigate knee degeneration of non-amputee [17]. Thus, this keel design may enable amputees who experience intact knee osteoarthritis to more effectively offload their intact knee.

Limitations and Future Work. Although the optimization framework successfully identified optimal foot designs, there are potential limitations and areas of future work. First, the observed influence of the different stiffness profiles on muscle and foot function need to be experimentally verified. Thus, future work should involve manufacturing the optimized ESAR feet and clinically testing them on amputees. Secondly, when reducing both metabolic cost and intact knee contact forces, we assumed an equal cost of these objectives. Changing the relative costs of these dual objectives may yield a wider range of designs to be analyzed
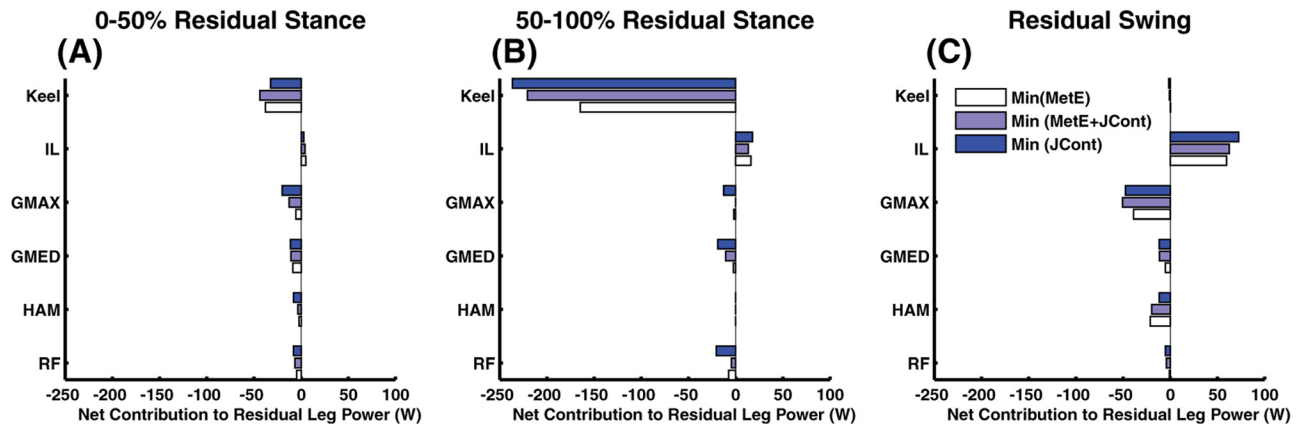
Fig. 9 Mean prosthetic foot and residual leg muscle contributions to total power delivered to the residual leg. Data were averaged during the first (left column) and second (middle column) halves of residual leg stance and swing (right column).

in the future. In addition, it is unclear whether the biomechanical objectives optimized in this study may be utilized by the central nervous system to optimize walking in a similar manner. However, as previously described, reducing metabolic cost and intact knee contact forces are important clinically-relevant objectives that hold promise for improving amputee mobility. While this framework is theoretical in nature, the simulated motions and muscle excitations emulated well experimentally-collected data of amputee walking, and the identified intact and residual leg muscle contributions to walking subtasks were consistent with previous studies of non-amputee walking [10,12,13,45]. In addition, the observed functions of the prosthetic keel to body support and forward propulsion during the first and second halves of stance as well as energy absorbed from the leg were consistent with the functional role of SOL in non-amputee walking [10]. Thus, the optimized movements were realistic, and the identified muscle and foot functions were found to be consistent with previous work. Furthermore, modeling assumptions were made such as the omission of the residual leg gastrocnemius and the rigid connection between the residual leg and prosthesis. The potential contribution of the residual leg gastrocnemius to walking subtasks would depend on limb length, etiology, surgical technique and the amount of muscle atrophy. In addition, the biomechanical functions of this muscle were likely captured by the residual leg biceps femoris short head, which was included in our model and found to have small contributions to the overall walking mechanics. Prosthesis fit is another important factor that was difficult to incorporate in the model since it depends on the type of socket-residual limb interface (e.g., pin-lock versus a vacuum suspension system) as well as the quality of the interface. Future experimental studies are needed to characterize these factors prior to incorporating them in the musculoskeletal model. Finally, a 2D model was used in this study due to the computational intensity of the analyses. With future increases in computational speed and optimization algorithm efficiency, 3D studies should be performed to identify muscle and foot function in the non-sagittal planes of motion.

Conclusions

In summary, fine-tuning the nominal SLS ESAR prosthetic foot design by stiffening the toe and mid-foot while making the ankle and heel less stiff may improve ESAR foot performance by offloading the intact knee during early to mid-stance of the intact leg and reducing the metabolic cost of intact and residual leg muscles over the gait cycle. In addition, minimizing only metabolic cost or only intact knee contact force resulted in muscle and prosthetic foot compensations that adversely increased the opposing objective, while minimizing both objectives simultaneously incorporated common foot stiffness characteristics (e.g., increasing toe

stiffness when reducing intact knee contact force and decreasing ankle stiffness when reducing metabolic cost). By coupling detailed modeling and design optimization of ESAR prosthetic feet with musculoskeletal modeling and forward dynamics simulations, this study provided an important first step in optimizing the stiffness characteristics of ESAR prosthetic feet to improve amputee mobility and has provided insight into the influence of foot stiffness on foot and muscle function, metabolic cost, and intact knee contact forces.

References

[1] Sanderson, D. J., and Martin, P. E., 1997, "Lower Extremity Kinematic and Kinetic Adaptations in Unilateral Below-Knee Amputees During Walking," Gait and Posture, **6**, pp. 126–136.
[2] Winter, D. A., and Sienko, S. E., 1988, "Biomechanics of Below-Knee Amputee Gait," J. Biomech., **21**(5), pp. 361–367.
[3] Waters, R. L., Perry, J., Antonelli, D., and Hislop, H., 1976, "Energy Cost of Walking of Amputees: The Influence of Level of Amputation," J. Bone Jt. Surg. Am., **58**(1), pp. 42–46. Available at http://www.ncbi.nlm.nih.gov/pubmed/1249111
[4] Robinson, J. L., Smidt, G. L., and Arora, J. S., 1977, "Accelerographic, Temporal, and Distance Gait Factors in Below-Knee Amputees," Phys. Ther., **57**(8), pp. 898–904. Available at http://www.ncbi.nlm.nih.gov/pubmed/877157
[5] Kulkarni, J., Gaine, W. J., Buckley, J. G., Rankine, J. J., and Adams, J., 2005, "Chronic Low Back Pain in Traumatic Lower Limb Amputees," Clin. Rehabil., **19**(1), pp. 81–86.
[6] Ephraim, P. L., Wegener, S. T., Mackenzie, E. J., Dillingham, T. R., and Pezzin, L. E., 2005, "Phantom Pain, Residual Limb Pain, and Back Pain in Amputees: Results of a National Survey," Arch. Phys. Med. Rehabil., **86**(10), pp. 1910–1919.
[7] Smith, D. G., Ehde, D. M., Legro, M. W., Reiber, G. E., Del Aguila, M., and Boone, D. A., 1999, "Phantom Limb, Residual Limb, and Back Pain After Lower Extremity Amputations," Clin. Orthop. Relat. Res., **361**, pp. 29–38.
[8] Burke, M. J., Roman, V., and Wright, V., 1978, "Bone and Joint Changes in Lower Limb Amputees," Ann. Rheum. Dis., **37**(3), pp. 252–254.
[9] Gailey, R., Allen, K., Castles, J., Kucharik, J., and Roeder, M., 2008, "Review of Secondary Physical Conditions Associated With Lower-Limb Amputation and Long-Term Prosthesis Use," J. Rehabil. Res. Dev., **45**(1), pp. 15–29.
[10] Neptune, R. R., Kautz, S. A., and Zajac, F. E., 2001, "Contributions of the Individual Ankle Plantar Flexors to Support, Forward Progression and Swing Initiation During Walking," J. Biomech., **34**(11), pp. 1387–1398.
[11] Hafner, B. J., Sanders, J. E., Czerniecki, J. M., and Fergason, J., 2002, "Transtibial Energy-Storage-and-Return Prosthetic Devices: A Review of Energy Concepts and a Proposed Nomenclature," J. Rehabil. Res. Dev., **39**(1), pp. 1–11. Available at http://www.ncbi.nlm.nih.gov/pubmed/11926321
[12] Liu, M. Q., Anderson, F. C., Pandy, M. G., and Delp, S. L., 2006, "Muscles That Support the Body Also Modulate Forward Progression During Walking," J. Biomech., **39**(14), pp. 2623–2630.

[13] Neptune, R. R., Zajac, F. E., and Kautz, S. A., 2004, "Muscle Force Redistributes Segmental Power for Body Progression During Walking," Gait and Posture, **19**(2), pp. 194–205.

[14] Neptune, R. R., and Kautz, S. A., 2000, "Knee Joint Loading in Forward versus Backward Pedaling: Implications for Rehabilitation Strategies," Clin. Biomech. (Bristol, Avon), **15**(7), pp. 528–535.

[15] Sasaki, K., Neptune, R. R., and Kautz, S. A., 2009, "The Relationships Between Muscle, External, Internal and Joint Mechanical Work During Normal Walking," J. Exp. Biol., **212**(Pt 5), pp. 738–744.

[16] Sasaki, K., and Neptune, R. R., 2010, "Individual Muscle Contributions to the Axial Knee Joint Contact Force During Normal Walking," J. Biomech., **43**(14), pp. 2780–2784.

[17] Shelburne, K. B., Torry, M. R., and Pandy, M. G., 2005, "Muscle, Ligament, and Joint-Contact Forces at the Knee During Walking," Med. Sci. Sports Exercise, **37**(11), pp. 1948–1956.

[18] Umberger, B. R., 2010, "Stance and Swing Phase Costs in Human Walking," J. R. Soc., Interface, **7**(50), pp. 1329–1340.

[19] Fey, N. P., Klute, G. K., and Neptune, R. R., 2011, "The Influence of Energy Storage and Return Foot Stiffness on Walking Mechanics and Muscle Activity in Below-Knee Amputees," Clin. Biomech. (Bristol, Avon), **26**(10), pp. 1025–1032.

[20] Ventura, J. D., Klute, G. K., and Neptune, R. R., 2011, "The Effects of Prosthetic Ankle Dorsiflexion and Energy Return on Below-Knee Amputee Leg Loading," Clin. Biomech. (Bristol, Avon), **26**(3), pp. 298–303.

[21] Ventura, J. D., Klute, G. K., and Neptune, R. R., 2011, "The Effect of Prosthetic Ankle Energy Storage and Return Properties on Muscle Activity in Below-Knee Amputee Walking," Gait and Posture, **33**(2), pp. 220–226.

[22] Zmitrewicz, R. J., Neptune, R. R., and Sasaki, K., 2007, "Mechanical Energetic Contributions From Individual Muscles and Elastic Prosthetic Feet During Symmetric Unilateral Transtibial Amputee Walking: A Theoretical Study," J. Biomech., **40**(8), pp. 1824–1831.

[23] Delp, S. L., Loan, J. P., Hoy, M. G., Zajac, F. E., Topp, E. L., and Rosen, J. M., 1990, "An Interactive Graphics-Based Model of the Lower Extremity to Study Orthopaedic Surgical Procedures," IEEE Trans. Biomed. Eng., **37**(8), pp. 757–767.

[24] Mattes, S. J., Martin, P. E., and Royer, T. D., 2000, "Walking Symmetry and Energy Cost in Persons With Unilateral Transtibial Amputations: Matching Prosthetic and Intact Limb Inertial Properties," Arch. Phys. Med. Rehabil., **81**(5), pp. 561–568.

[25] Yamaguchi, G. T., and Zajac, F. E., 1989, "A Planar Model of the Knee Joint to Characterize the Knee Extensor Mechanism," J. Biomech., **22**(1), pp. 1–10.

[26] Neptune, R. R., Wright, I. C., and Van Den Bogert, A. J., 2000, "A Method for Numerical Simulation of Single Limb Ground Contact Events: Application to Heel-Toe Running," Comput. Methods Biomech. Biomed. Eng., **3**(4), pp. 321–334.

[27] Anderson, F. C., and Pandy, M. G., 1999, "A Dynamic Optimization Solution for Vertical Jumping in Three Dimensions," Comput. Methods Biomech. Biomed. Eng., **2**(3), pp. 201–231.

[28] Davy, D. T., and Audu, M. L., 1987, "A Dynamic Optimization Technique for Predicting Muscle Forces in the Swing Phase of Gait," J. Biomech., **20**(2), pp. 187–201.

[29] Hall, A. L., Peterson, C. L., Kautz, S. A., and Neptune, R. R., 2011, "Relationships Between Muscle Contributions to Walking Subtasks and Functional Walking Status in Persons With Post-Stroke Hemiparesis," Clin. Biomech. (Bristol, Avon), **26**(5), pp. 509–515.

[30] Zajac, F. E., 1989, "Muscle and Tendon: Properties, Models, Scaling, and Application to Biomechanics and Motor Control," Crit. Rev. Biomed. Eng., **17**(4), pp. 359–411. Available at http://www.ncbi.nlm.nih.gov/pubmed/2676342

[31] Raasch, C. C., Zajac, F. E., Ma, B., and Levine, W. S., 1997, "Muscle Coordination of Maximum-Speed Pedaling," J. Biomech., **30**(6), pp. 595–602.

[32] Winters, J. M., and Stark, L., 1988, "Estimated Mechanical Properties of Synergistic Muscles Involved in Movements of a Variety of Human Joints," J. Biomech., **21**(12), pp. 1027–1041.

[33] Umberger, B. R., Gerritsen, K. G., and Martin, P. E., 2003, "A Model of Human Muscle Energy Expenditure," Comput. Methods Biomech. Biomed. Eng., **6**(2), pp. 99–111.

[34] South, B. J., Fey, N. P., Bosker, G., and Neptune, R. R., 2010, "Manufacture of Energy Storage and Return Prosthetic Feet Using Selective Laser Sintering," J. Biomech. Eng., **132**(1), p. 015001.

[35] Goffe, W. L., Ferrier, G. D., and Rogers, J., 1994, "Global Optimization of Statistical Functions With Simulated Annealing," J. Econometr., **60**(1–2), pp. 65–99.

[36] Silverman, A. K., Fey, N. P., Portillo, A., Walden, J. G., Bosker, G., and Neptune, R. R., 2008, "Compensatory Mechanisms in Below-Knee Amputee Gait in Response to Increasing Steady-State Walking Speeds," Gait and Posture, **28**(4), pp. 602–609.

[37] Neptune, R. R., Sasaki, K., and Kautz, S. A., 2008, "The Effect of Walking Speed on Muscle Function and Mechanical Energetics," Gait and Posture, **28**(1), pp. 135–143.

[38] Fregly, B. J., and Zajac, F. E., 1996, "A State-Space Analysis of Mechanical Energy Generation, Absorption, and Transfer During Pedaling," J. Biomech., **29**(1), pp. 81–90.

[39] Kim, H. J., Fernandez, J. W., Akbarshahi, M., Walter, J. P., Fregly, B. J., and Pandy, M. G., 2009, "Evaluation of Predicted Knee-Joint Muscle Forces During Gait Using an Instrumented Knee Implant," J. Orthop. Res., **27**(10), pp. 1326–1331.

[40] Lin, Y. C., Walter, J. P., Banks, S. A., Pandy, M. G., and Fregly, B. J., 2010, "Simultaneous Prediction of Muscle and Contact Forces in the Knee During Gait," J. Biomech., **43**(5), pp. 945–952.

[41] Astephen, J. L., Deluzio, K. J., Caldwell, G. E., Dunbar, M. J., and Hubley-Kozey, C. L., 2008, "Gait and Neuromuscular Pattern Changes are Associated With Differences in Knee Osteoarthritis Severity Levels," J. Biomech., **41**(4), pp. 868–876.

[42] Childs, J. D., Sparto, P. J., Fitzgerald, G. K., Bizzini, M., and Irrgang, J. J., 2004, "Alterations in Lower Extremity Movement and Muscle Activation Patterns in Individuals With Knee Osteoarthritis," Clin. Biomech. (Bristol, Avon), **19**(1), pp. 44–49.

[43] Deluzio, K. J., and Astephen, J. L., 2007, "Biomechanical Features of Gait Waveform Data Associated With Knee Osteoarthritis: An Application of Principal Component Analysis," Gait and Posture, **25**(1), pp. 86–93.

[44] Zeni, J. A., Jr., and Higginson, J. S., 2009, "Differences in Gait Parameters Between Healthy Subjects and Persons With Moderate and Severe Knee Osteoarthritis: A Result of Altered Walking Speed?," Clin. Biomech. (Bristol, Avon), **24**(4), pp. 372–378.

[45] Anderson, F. C., and Pandy, M. G., 2003, "Individual Muscle Contributions to Support in Normal Walking," Gait and Posture, **17**(2), pp. 159–169.